Determination of hydrogen exchange and relaxation parameters in PHIP complexes at micromolar concentrations

Lisanne Sellies[1], Ruud L. E. G. Aspers[1], and Marco Tessari[1]

[1]Institute for Molecules and Materials, Radboud University, Nijmegen, 6525AJ, the Netherlands

Correspondence to: Marco Tessari (m.tessari@science.ru.nl)

Abstract. Non-hydrogenative Para-Hydrogen Induced Polarization (PHIP) is a fast, efficient and relatively inexpensive approach to enhance Nuclear Magnetic Resonance (NMR) signals of small molecules in solution. The efficiency of this technique depends on the interplay of NMR relaxation and kinetic processes, which, at high concentrations, can be characterized by selective inversion experiments. However, in the case of dilute solutions this approach is clearly not viable. Here, we present alternative PHIP-based NMR experiments to determine hydrogen and hydrides' relaxation parameters as well as the rate constants for para-hydrogen association to and dissociation from asymmetric PHIP complexes at micromolar concentrations. Access to these parameters is necessary to understand and improve the PHIP enhancements of (dilute) substrates present in, for instance, biofluids and natural extracts.

1 Introduction

The intrinsically low sensitivity of magnetic resonance techniques is a strong limitation to their application in fields such as chemical analysis, metabolic imaging and biomarkers identification. Several hyperpolarization methods have been developed to overcome this issue, including dynamic nuclear polarization, (Ardenkjær-Larsen et al., 2003) spin exchange optical pumping (Walker and Happer, 1997) and Para-Hydrogen Induced Polarization (PHIP) (Bowers and Weitekamp, 1987; Pravica and Weitekamp, 1988). Particularly, PHIP has grown into a versatile technique since the recent discovery of non-hydrogenative routes to achieve nuclear spin hyperpolarization (Adams et al., 2009). Figure 1 sketches the core of a typical non-hydrogenative PHIP-machinery, based on the reversible association of para-hydrogen (p-H_2) and substrates to an iridium-catalyst. We have previously demonstrated that a large excess of a suitable metal ligand (e.g. 1-methyl-1,2,3-triazole (mtz)), referred to as "co-substrate" in the following, is necessary to preserve the efficiency of non-hydrogenative PHIP when the substrate under investigation is highly dilute (Eshuis et al., 2014; Eshuis et al., 2015).

In Fig. 1a, the Signal Amplification By Reversible Exchange (SABRE) (Adams et al., 2009) technique is sketched: at low magnetic field, the scalar coupling network within the transient complex allows the spontaneous transfer of spin order from the hydrides (derived from p-H_2 binding) to the nuclear spins of the substrate molecules. Subsequent complex dissociation releases hyperpolarized substrate molecules in solution, which can be detected with several orders of magnitude enhanced Nuclear Magnetic Resonance (NMR) sensitivity (Theis et al., 2015; Rayner et al., 2017; Rayner and Duckett, 2018; Iali et al., 2019; Gemeinhardt et al., 2020).

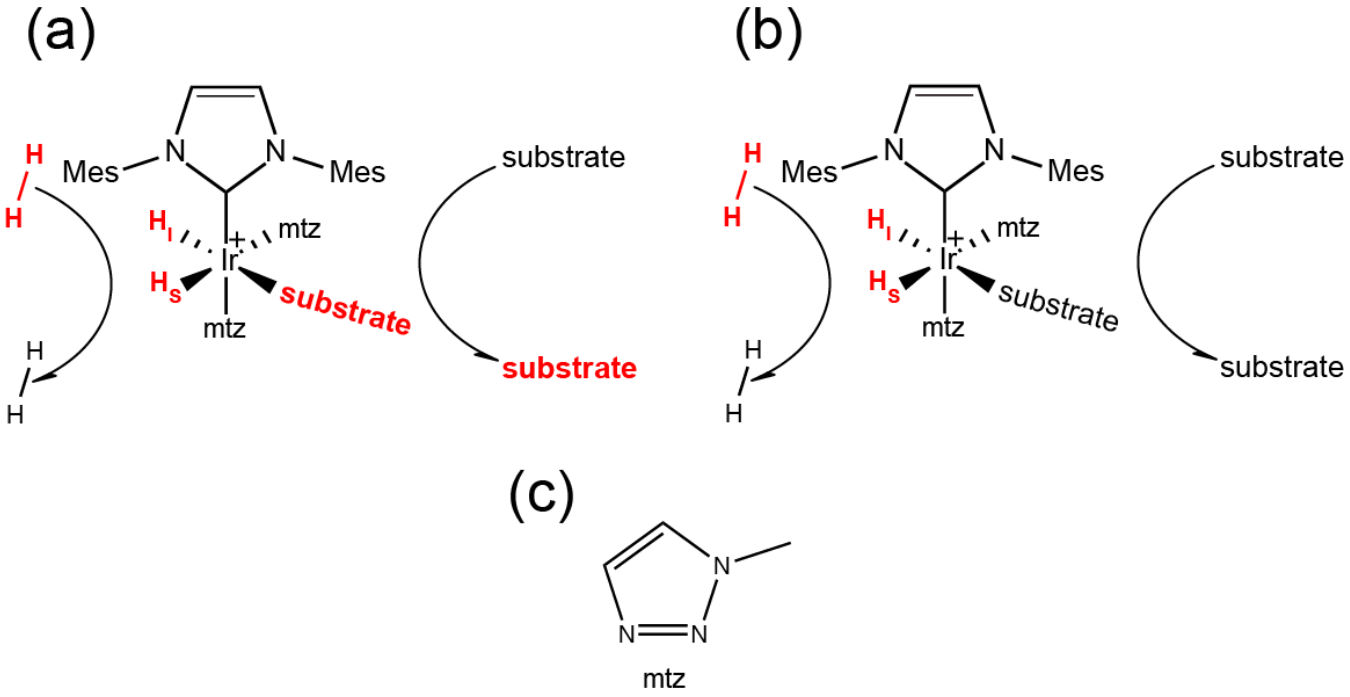

Figure 1: (a) Schematic representation of the SABRE experiment at low magnetic field: spontaneous transfer of spin order from the hydrides originating from p-H_2 to the substrate nuclear spins occurs via the scalar coupling network within the transient complex [Ir(IMes)$(H)_2$(substrate)$(mtz)_2$]Cl. The subsequent dissociation of the substrate produces hyperpolarized molecules in solution that can be detected by NMR with enhanced sensitivity. SABRE hyperpolarization has been demonstrated for different classes of compounds (e.g. nitrogen (Adams et al., 2009) and sulphur (Shchepin et al., 2016) heteroaromatic compounds, nitriles (Mewis et al., 2015), amines (Iali et al., 2018), Schiff bases (Logan et al., 2016) and diazirines (Theis et al., 2016)). (b) Schematic representation of PHIP at high magnetic field: formation of the asymmetric complex [Ir(IMes)$(H)_2$(substrate)$(mtz)_2$]Cl due to the reversible association of p-H_2 and substrates produces longitudinal spin order of the hydrides, which can be revealed by NMR signals that are enhanced up to three orders of magnitude compared to thermal measurements on a conventional high field spectrometer. (c) Structure of the mtz co-substrate (1-methyl-1,2,3-triazole).

Alternatively, the transient complex itself offers the possibility to investigate the substrates bound to the catalyst (see Fig. 1b). We have previously demonstrated that such an asymmetric complex is an ideal NMR-chemosensor (Hermkens et al., 2016; Sellies et al., 2019): molecules capable of associating to the PHIP catalyst can be probed by a pair of hydrides signals enhanced by ca. three orders of magnitude with respect to thermal NMR measured at 500 MHz. This allows the detection and quantification of substrates present at sub-micromolar concentrations in complex mixtures (Eshuis et al., 2015), such as biofluids (Reile et al., 2016; Sellies et al., 2019) and natural extracts (Hermkens et al., 2016; Hermkens et al., 2018).

The NMR signal enhancements obtained by these reversible PHIP techniques result from a complex interplay of substrate exchange, para-hydrogen exchange and relaxation processes (Barskiy et al., 2016; Stanbury et al., 2019). For instance, at high field, the singlet state of para-hydrogen associating to an asymmetric complex rapidly turns into hydrides' longitudinal spin order, which can be converted into enhanced hydrides magnetization by a SEPP pulse sequence (Sengstschmid, 1996). The resulting hydrides' signal enhancement depends, therefore, amongst others, on the para-hydrogen lifetime in solution, the rates of para-hydrogen association/dissociation to/from the complex and the NMR relaxation of the longitudinal spin

order in the complex. Gaining access to these parameters is crucial in order to rationalize the observed variations in hydrides' NMR signal enhancement for different substrates (Sellies et al., 2019) or to optimally tune the chemosensing system (e.g. select the best co-substrate molecule) for specific substrates and/or experimental applications. Since some of these parameters, e.g. the hydrogen dissociation rate constant, strongly depend on the concentration of ligands in solution (Cowley et al., 2011; Appleby et al., 2015), it is important to measure them in the same dilute conditions normally encountered in PHIP-NMR.

The association and dissociation rates of hydrogen and substrates to/from the iridium complex can be determined using exchange NMR spectroscopy (EXSY), in which, for instance, the longitudinal magnetization of one of the two exchanging forms is selectively inverted and probed together with its exchange product after different durations of a mixing time (Cowley et al., 2011; Appleby et al., 2015). These experiments are typically performed at high concentrations of substrate and catalyst, making them unsuitable for characterizing low concentrated complexes. Instead, the hyperpolarization provided by para-hydrogen can be exploited, as we previously demonstrated for the measurement of the substrate dissociation rate from asymmetric complexes (Hermkens et al., 2017).

Here, we present two PHIP-NMR experiments to characterize the hydrides' dynamics in these asymmetric complexes at low concentration. The analysis of the resulting NMR data provides not only the hydrogen exchange rates in the low μM regime, but also the hydrides' relaxation parameters. We illustrate this approach for the asymmetric complex formed upon binding of the substrate isoquinoline (IQ) to the Ir-IMes catalyst in the presence of an excess of mtz as co-substrate.

2 Material and methods

2.1 Chemicals

Complex precursor [IrCl(COD)(IMes)] (IMes = 1,3-bis(2,4,6-trimethylphenyl)imidazole-2-ylidene; COD = cyclooctadiene) and co-substrate mtz were synthesized according to published methods (Kelly et al., 2008; Seefeld et al., 2008). Isoquinoline and methanol-d_4 were purchased from Sigma-Aldrich and used as supplied. Para-hydrogen (p-H_2) was produced with an in-house designed generator (Cryoworld B.V., The Netherlands) consisting of a 2 L vessel embedded in a liquid nitrogen bath. Normal hydrogen (purity 5.0) at 40 bar was cooled down to 77 K in the presence of 100 ml of 4–8 MESH charcoal (Sigma-Aldrich). The resulting 51% p-H_2 was transferred into an aluminum cylinder (Nitrous Oxides Systems, Holley Performance Products, USA) (Feng et al., 2012) and connected to a setup for gas-liquid reactions (Eshuis et al., 2015), as sketched in Appendix A.

2.2 Sample preparation and setup

[IrCl(COD)(IMes)], mtz and isoquinoline were mixed to a final concentration of 0.8 mM, 15 mM and 50 μM in methanol-d_4, respectively. The solution was transferred into a 5 mm quick pressure valve (QPV) NMR tube (Wilmad-LabGlass). This tube was sealed with an in-house built headpiece to which three PEEK tube lines are connected (see Appendix A). Nitrogen

gas was passed through the solution to remove dissolved oxygen, after which [IrCl(COD)(IMes)] was hydrogenated (activated) by bubbling p-H_2 through the solution for 1.5 seconds every two minutes for approximately 30 minutes.

2.3 p-H_2 supply

At the beginning of each transient of an NMR experiment the sample tube was depressurized to 4 bar through a vent line (250 ms), after which p-H_2 at 5 bar pressure was supplied for 1.5 s through a line ending at the bottom of the NMR tube. Back pressure was applied to quickly stop the bubbling (250 ms), followed by a recovery delay of 500 ms prior to the NMR pulse sequence. The vent-, bubble-, and back pressure delays are spectrometer-controlled through solenoid valves connected to the console (see Appendix A).

2.4 NMR experiments

All NMR experiments were performed at 25 °C on an Agilent Unity INOVA spectrometer operating at 500 MHz ^{1}H resonance frequency, using a cryo-cooled HCN triple-resonance probe equipped with z-pulsed field gradients.

The datasets employed in this study consist of series of 18 1D PHIP-NMR spectra acquired with variable exchange/relaxation periods Δ ranging between 100 ms and 5 s. The transmitter offset was placed at -11.35 ppm, and the spectral region between -31.36 ppm and 8.66 ppm was acquired for 0.5 seconds. 4 or 8 transients were recorded per each Δ duration corresponding to an experimental time of 10 or 20 minutes for a complete series. In order to avoid variations in the level of p-H_2 in solution, the time interval between two successive bubbling periods (at the beginning of each transient) was maintained constant, independent of the duration of Δ.

The decay rate of p-H_2 in solution was determined in a separate experiment, by acquiring a series of 48 single-scan 1D PHIP-NMR signals of the high-field hydride in the asymmetric complex formed by isoquinoline, mtz and the iridium catalyst. After bubbling p-H_2 in solution at the beginning of the experiment, all spectra were acquired (one per second) without refreshing p-H_2 during the measurement. As the p-H_2 concentration in solution decreases, the PHIP-enhancement of the NMR hydrides signals drops. The rate constant of the conversion of para-enriched H_2 to thermal hydrogen was obtained by the exponential fit of the signal integral versus time.

All data sets were processed with nmrPipe (Delaglio et al., 1995) and analyzed with iNMR (Balacco and Marino, 2016) using 90-degree shifted squared sine-bell apodization, prior to zero filling to 128k complex points, and Fourier transformation. The fitting of NMR signal integrals versus exchange/relaxation time Δ was performed using in-house written routines implemented in Octave (Eaton et al., 2009).

3 Theory

3.1 PHIP-NMR pulse sequences for hydrogen kinetics/relaxation

At high magnetic field the two hydrides of asymmetric Ir-IMes complexes (see Fig. 1) are not chemically equivalent, which, due to the distribution of complexes' formation in time, causes efficient conversion of the singlet state originating from p-H_2 to longitudinal spin order (Buljubasich et al., 2013). We have previously demonstrated that this spin order can be converted into enhanced magnetization, allowing the NMR detection of hydrides signals down to sub-micromolar complex concentrations (Eshuis et al., 2015; Sellies et al., 2019). This sensitivity increase can also be used to study the exchange of p-H_2 in the iridium catalyst as well as the NMR relaxation of the hydrides and p-H_2 in solution.

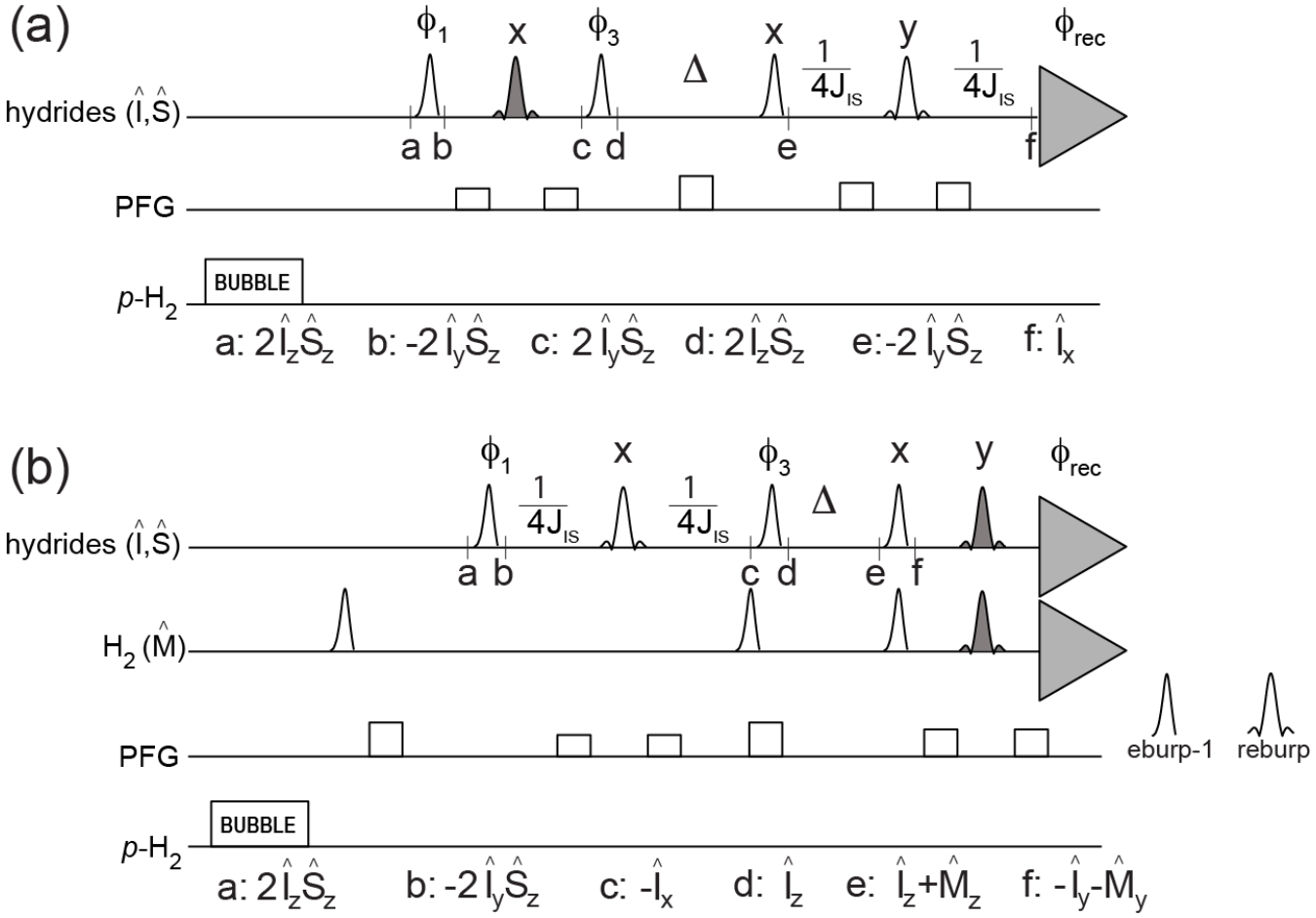

Figure 2. Pulse sequences to measure relaxation and kinetic parameters for hydrides in asymmetric complexes. The transmitter offset is placed at -11.35 ppm, and the spectral region between -31.36 ppm and 8.66 ppm is acquired. Open shaped profiles indicate selective off-resonance pulses *eburp-1* (for excitation of the high-field hydride, 500 Hz bandwidth) or *reburp* (for refocusing, 2000 Hz bandwidth). Filled *reburp* pulses cover a smaller bandwidth (500 Hz) for the hydrogen and/or the high-field hydride resonance. Individual scans are stored separately and recombined during processing so that different pathways can be selected. J_{IS} indicates

the inter-hydrides scalar coupling constant (8.2 Hz). (a) Pulse scheme to measure the decay rate of hydrides' longitudinal spin order as well as association of p-H_2 to the iridium complex. The following phase cycle is employed: ϕ_1 = x,-x; ϕ_3 = x,x,-x,-x; ϕ_{rec} = x. (b) Pulse scheme to measure the decay rate of hydrides' longitudinal magnetization as well as hydrides dissociation from the complex. The following phase cycle is employed: ϕ_1 = x,-x; ϕ_3 = y,y,-y,-y; ϕ_{rec} = x,-x,-x,x. H_2 longitudinal magnetization is suppressed at the start of the pulse sequence by selective 90-degree pulses after the bubbling period and at the beginning of the relaxation period Δ. The final excitation/spin-echo before acquisition selectively excites/refocuses both the magnetization from H_2 and from the high-field hydride. In other words, the last excitation/refocusing pulses consist of the superposition of two *eburp-1*/*reburp* pulses, for the selective detection of the high-field hydride as well as the hydrogen resonances.

The pulse schemes in Fig. 2 make use of PHIP-NMR to quantitatively characterize these kinetic and relaxation parameters for asymmetric complexes at low micromolar concentration, i.e. the conditions in which p-H_2 hyperpolarization is typically used for the detection of dilute substrates. The relevant spin operators at specified time points in the pulse schemes are indicated.

The experiment sketched in Fig. 2a can monitor p-H_2 association as well as the decay of the hydrides' spin order as a function of the delay time Δ. The first spin echo (between time-points *a* and *d*) allows implementing a phase cycle to separate the hydrides signals produced by p-H_2 association to the complex during the bubbling period from those resulting from p-H_2 association during the exchange/relaxation period Δ. After the time Δ the spin order is converted to antiphase magnetization, refocused and acquired. By storing each individual scan separately it is then possible to monitor either the hydrides decay, or the association of p-H_2 to the complex during Δ, by taking different combinations of the acquired signals (e.g. multiplying some scans by -1 before adding them together, corresponding to a 180° phase shift of the receiver).

The pulse scheme in Fig. 2b was used to monitor the decay of the hydrides' longitudinal magnetization as well as the hydrides' dissociation to produce hyperpolarized hydrogen in solution as a function of the mixing time Δ. After the bubbling period, the hydrides' spin order is converted to antiphase magnetization, refocused and stored as longitudinal magnetization during the exchange/relaxation time Δ. After this time, the remaining hydrides' magnetization as well as the transferred hydrogen magnetization are excited and acquired simultaneously, in the same spectrum.

3.2 Spin Dynamics

The evolution of the hydrides' magnetization/spin order during the relaxation/exchange time Δ is described by the equations below:

$$\frac{d}{dt}\begin{bmatrix} \left\langle \left(2\hat{I}_z\hat{S}_z\right)^B \right\rangle \\ \left\langle \left(2\hat{I}_z\hat{S}_z\right)^F \right\rangle \end{bmatrix} = -\begin{bmatrix} \left(k^*_{diss} + \rho^{so}_{hydr}\right) & -k^*_{ass} \\ -k^*_{diss} & \left(k^*_{ass} + \rho_{pH_2}\right) \end{bmatrix} \begin{bmatrix} \left\langle \left(2\hat{I}_z\hat{S}_z\right)^B \right\rangle \\ \left\langle \left(2\hat{I}_z\hat{S}_z\right)^F \right\rangle \end{bmatrix} \quad (1)$$

$$\frac{d}{dt}\begin{bmatrix} \left\langle \left(\hat{I}_z\right)^B \right\rangle \\ \left\langle \left(\hat{I}_z\right)^F \right\rangle \end{bmatrix} = -\begin{bmatrix} \left(k^*_{diss} + \rho_{hydr}\right) & -k^*_{ass} \\ -k^*_{diss} & \left(k^*_{ass} + \rho_{H_2}\right) \end{bmatrix} \begin{bmatrix} \left\langle \left(\hat{I}_z\right)^B \right\rangle - \hat{I}^B_{eq} \\ \left\langle \left(\hat{I}_z\right)^F \right\rangle - \hat{I}^F_{eq} \end{bmatrix} \quad (2)$$

Equation (1) describes the kinetics and NMR relaxation of the longitudinal spin order of hydrides (index "B") and of free hydrogen (index "F"). Here, k^*_{diss} and k^*_{ass} represent the dissociation and association rate constants of hydrogen from/to the asymmetric Ir-IMes complexes, ρ^{so}_{hydr} the relaxation of hydrides' longitudinal spin order in these complexes and ρ_{pH_2} the rate of thermalization of para-enriched H_2. The asterisk marking the kinetic rate constants indicates that they most likely result from multi-step processes and their physical interpretation strictly depends on the hypothesized mechanism. Note that the (unobservable) term $\left(2\hat{I}_z\hat{S}_z\right)^F$ refers here to both p-H_2 as well as the longitudinal spin order of free hydrogen (Barskiy et al., 2019). Analogously, Eq. (2) describes the dynamics of the longitudinal magnetization of hydrides and free hydrogen in solution; in this case the kinetic processes involved are identical, while ρ_{hydr} and ρ_{H_2} refer to the spin-lattice relaxation rates of the hydrides and of free hydrogen, respectively. Note that in the presence of cross-correlated relaxation mechanisms, the dynamics of $\left\langle \hat{I}_z \right\rangle$ and $\left\langle 2\hat{I}_z\hat{S}_z \right\rangle$ are coupled and are not described by two independent equations (Eq. (1) and Eq. (2)). In the present case, however, such cross terms are likely to be negligible and their effect has not been considered.

It should be mentioned that in principle also substrate and co-substrate dissociation might contribute to the decay of the hydrides magnetization and spin order ($\left\langle \left(\hat{I}_z\right)^B \right\rangle$ and $\left\langle \left(2\hat{I}_z\hat{S}_z\right)^B \right\rangle$). These additional processes can be easily followed as they produce a magnetization transfer from the high-field to the low-field hydride or to the hydrides of the symmetric complex ($[Ir(IMes)(H)_2(mtz)_3]^+$). However, in the present case such transfer was not observed, indicating that these exchange processes occur at a significantly lower rate than the hydrides' relaxation for the complex here investigated. Therefore, the decay rates of the hydrides (ρ_{hydr} and ρ^{so}_{hydr}) determined in this work correspond to NMR relaxation parameters to a very good approximation.

The solution of Eq. (1) refers here only to the dynamics of the hydrides' longitudinal spin order, as the corresponding term for free hydrogen is not observable:

$$\left\langle \left(2\hat{I}_z\hat{S}_z\right)^B \right\rangle(\Delta) = \frac{e^{-\left(\bar{\rho}^{so}+\bar{k}\right)\Delta}}{1+\frac{\left(\bar{k}^2-\Delta k^2\right)}{\left(\Delta\rho^{so}+\Delta k+\varepsilon^{so}\right)^2}} \left\{ \left(e^{-\varepsilon^{so}\Delta} + \frac{\left(\bar{k}^2-\Delta k^2\right)}{\left(\Delta\rho^{so}+\Delta k+\varepsilon^{so}\right)^2} e^{\varepsilon^{so}\Delta} \right) \left\langle \left(2\hat{I}_z\hat{S}_z\right)^B \right\rangle(0) \right.$$
$$\left. + \frac{\left(\bar{k}-\Delta k\right)}{\left(\Delta\rho^{so}+\Delta k+\varepsilon^{so}\right)} \left(e^{\varepsilon^{so}\Delta} - e^{-\varepsilon^{so}\Delta}\right) \left\langle \left(2\hat{I}_z\hat{S}_z\right)^F \right\rangle(0) \right\} \quad (3)$$

$$\bar{\rho}^{so} = \frac{\rho^{so}_{hydr}+\rho_{pH_2}}{2} \qquad \Delta\rho^{so} = \frac{\rho^{so}_{hydr}-\rho_{pH_2}}{2} \qquad \bar{k} = \frac{k^*_{diss}+k^*_{ass}}{2} \qquad \Delta k = \frac{k^*_{diss}-k^*_{ass}}{2}$$

$$\varepsilon^{so} = \sqrt{\left(\Delta\rho^{so}+\Delta k\right)^2+\bar{k}^2-\Delta k^2}$$

By combining individual scans with coefficients {1,-1,-1,1}, it is possible to select the signal resulting from the hydrides associated to the complex during the bubbling period, while discarding the contribution originating from the association of p-H_2 during the time Δ. In this case, only the first term of Eq. (3) should be considered:

$$\left\langle \left(2\hat{I}_z\hat{S}_z\right)^B \right\rangle(\Delta) = \frac{e^{-\left(\bar{\rho}^{so}+\bar{k}\right)\Delta}}{1+\dfrac{\left(\bar{k}^2-\Delta k^2\right)}{\left(\Delta\rho^{so}+\Delta k+\varepsilon^{so}\right)^2}}\left(e^{-\varepsilon^{so}\Delta}+\frac{\left(\bar{k}^2-\Delta k^2\right)}{\left(\Delta\rho^{so}+\Delta k+\varepsilon^{so}\right)^2}e^{\varepsilon^{so}\Delta}\right)\left\langle \left(2\hat{I}_z\hat{S}_z\right)^B \right\rangle(0) \tag{4}$$

Equation (4) describes the decay of the hydrides' spin order due to NMR relaxation and dissociation of the hydrides from the complex. If, alternatively, individual scans are combined with coefficients {1,1,1,1}, only the signal originating from p-H_2 associating during the relaxation time Δ is observed. The time evolution of the measured signal is described by the second term of Eq. (3):

$$\left\langle \left(2\hat{I}_z\hat{S}_z\right)^B \right\rangle(\Delta) = \frac{e^{-\left(\bar{\rho}^{so}+\bar{k}\right)\Delta}}{1+\dfrac{\left(\bar{k}^2-\Delta k^2\right)}{\left(\Delta\rho^{so}+\Delta k+\varepsilon^{so}\right)^2}}\frac{\left(\bar{k}-\Delta k\right)}{\left(\Delta\rho^{so}+\Delta k+\varepsilon^{so}\right)}\left(e^{\varepsilon^{so}\Delta}-e^{-\varepsilon^{so}\Delta}\right)\left\langle \left(2\hat{I}_z\hat{S}_z\right)^F \right\rangle(0) \tag{5}$$

The time evolution of the longitudinal magnetization of free hydrogen and hydrides during the period Δ is given by the solution of Eq. (2):

$$\left\langle \left(\hat{I}_z\right)^B \right\rangle(\Delta) = \frac{e^{-\left(\bar{\rho}+\bar{k}\right)\Delta}}{1+\dfrac{\left(\bar{k}^2-\Delta k^2\right)}{\left(\Delta\rho+\Delta k+\varepsilon\right)^2}}\left\{\left(e^{-\varepsilon\Delta}+\frac{\left(\bar{k}^2-\Delta k^2\right)}{\left(\Delta\rho+\Delta k+\varepsilon\right)^2}e^{\varepsilon\Delta}\right)\left\langle \left(\hat{I}_z\right)^B \right\rangle(0)\right.$$
$$\left.+\frac{\left(\bar{k}-\Delta k\right)}{\left(\Delta\rho+\Delta k+\varepsilon\right)}\left(e^{\varepsilon\Delta}-e^{-\varepsilon\Delta}\right)\left\langle \left(\hat{I}_z\right)^F \right\rangle(0)\right\} \tag{6}$$

$$\left\langle \left(\hat{I}_z\right)^F \right\rangle(\Delta) = \frac{e^{-\left(\bar{\rho}+\bar{k}\right)\Delta}}{1+\dfrac{\left(\bar{k}^2-\Delta k^2\right)}{\left(\Delta\rho+\Delta k+\varepsilon\right)^2}}\left\{\frac{\left(\bar{k}+\Delta k\right)}{\left(\Delta\rho+\Delta k+\varepsilon\right)}\left(e^{\varepsilon\Delta}-e^{-\varepsilon\Delta}\right)\left\langle \left(\hat{I}_z\right)^B \right\rangle(0)\right.$$
$$\left.+\left(e^{\varepsilon\Delta}+\frac{\left(\bar{k}^2-\Delta k^2\right)}{\left(\Delta\rho+\Delta k+\varepsilon\right)^2}e^{-\varepsilon\Delta}\right)\left\langle \left(\hat{I}_z\right)^F \right\rangle(0)\right\} \tag{7}$$

$$\bar{\rho}=\frac{\rho_{hydr}+\rho_{H_2}}{2} \qquad \Delta\rho=\frac{\rho_{hydr}-\rho_{H_2}}{2} \qquad \bar{k}=\frac{k_{diss}+k_{ass}}{2^8} \qquad \Delta k=\frac{k_{diss}-k_{ass}}{2}$$
$$\varepsilon=\sqrt{\left(\Delta\rho+\Delta k\right)^2+\bar{k}^2-\Delta k^2}$$

In this case, both the bound form (i.e. the hydrides) and free hydrogen are observable. Since the phase cycle selects the signal originating from the hydrides associated to the complex during the bubbling period, while removing the contribution due to free hydrogen associating to the complex during Δ, the solution to Eq. (2) takes this form:

$$\left\langle \left(\hat{\mathrm{I}}_z\right)^{\mathrm{B}} \right\rangle (\Delta) = \frac{e^{-(\bar{\rho}+\bar{k})\Delta}}{1+\frac{\left(\bar{k}^2-\Delta k^2\right)}{\left(\Delta\rho+\Delta k+\varepsilon\right)^2}} \left(e^{-\varepsilon\Delta} + \frac{\left(\bar{k}^2-\Delta k^2\right)}{\left(\Delta\rho+\Delta k+\varepsilon\right)^2} e^{\varepsilon\Delta} \right) \left\langle \left(\hat{\mathrm{I}}_z\right)^{\mathrm{B}} \right\rangle (0) \qquad (8)$$

$$\left\langle \left(\hat{\mathrm{I}}_z\right)^{\mathrm{F}} \right\rangle (\Delta) = \frac{e^{-(\bar{\rho}+\bar{k})\Delta}}{1+\frac{\left(\bar{k}^2-\Delta k^2\right)}{\left(\Delta\rho+\Delta k+\varepsilon\right)^2}} \frac{\left(\bar{k}+\Delta k\right)}{\left(\Delta\rho+\Delta k+\varepsilon\right)} \left(e^{\varepsilon\Delta} - e^{-\varepsilon\Delta} \right) \left\langle \left(\hat{\mathrm{I}}_z\right)^{\mathrm{B}} \right\rangle (0) \qquad (9)$$

Note that in both expressions the contributions of thermal magnetization for hydrogen and hydrides are suppressed by the phase cycle.

4 Results and discussion

Previous studies (Cowley et al., 2011; Appleby et al., 2015) have clearly demonstrated the influence of substrates and catalyst concentrations on the hydrogen dissociation rate and, as a consequence, of the signal enhancement attainable via PHIP/SABRE. Therefore, in order to understand and improve the efficiency of PHIP for substrates in dilute asymmetric complexes, it is important to determine the relevant kinetic parameters at low concentrations. In the present study, isoquinoline at 50 μM concentration was used as a substrate together with mtz as co-substrate and iridium-IMes as metal complex. This combination of co-substrate and metal complex was previously utilized to detect dilute substrates in complex mixtures (Eshuis et al., 2014; Eshuis et al., 2015; Bordonali et al., 2019). The following experimental data, displayed in Fig. 3, were recorded using the two NMR experiments described above:

- the decay of hydrides longitudinal spin order as a function of the relaxation delay Δ (Fig. 3a, blue),
- the buildup of hydrides spin order due to association of p-H_2 to the complex as a function of the exchange delay Δ (Fig. 3a, green),
- the decay of hydrides magnetization as a function of the relaxation delay Δ (Fig. 3b, black),
- the buildup of H_2 magnetization resulting from hydrides dissociation as a function of the exchange delay Δ (Fig 3b, red).

The data were fitted simultaneously with the corresponding equations by optimization of the following parameters:

$$\rho_{hydr},\ \rho_{hydr}^{so},\ \rho_{\mathrm{H}_2},\ \rho_{p\mathrm{H}_2},\ k_{diss}^{*},\ k_{ass}^{*},\ \left\langle \left(2\hat{\mathrm{I}}_z\hat{\mathrm{S}}_z\right)^{\mathrm{F}} \right\rangle (0),\ \left\langle \left(2\hat{\mathrm{I}}_z\hat{\mathrm{S}}_z\right)^{\mathrm{B}} \right\rangle (0),\ \left\langle \left(\hat{\mathrm{I}}_z\right)^{\mathrm{B}} \right\rangle (0)$$

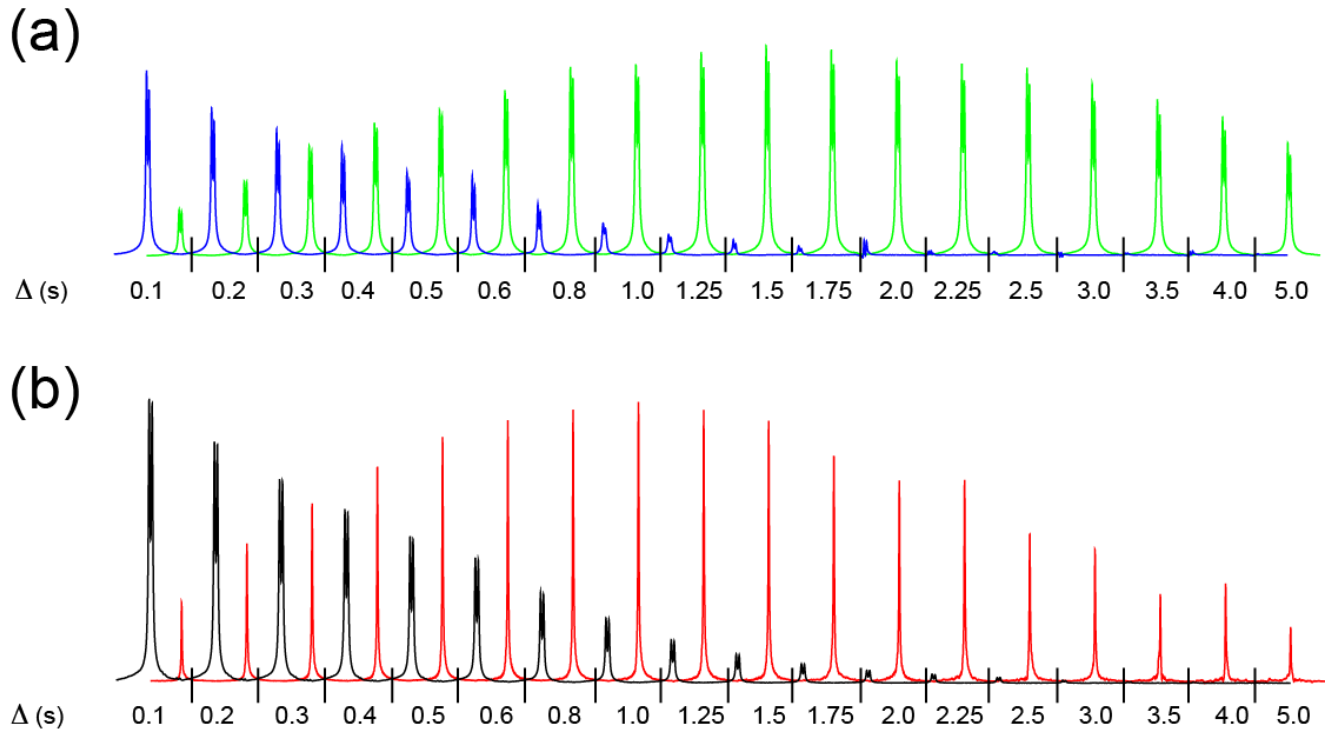

Figure 3. (a) High-field hydride signals obtained with the pulse sequence sketched in Fig. 2a, plotted as a function of the exchange/relaxation period Δ. The experiment monitors the decay of the longitudinal spin order of the hydrides or the association of p-H_2 to the complex during Δ. By taking different combinations of four FIDs as reported in Sec. 3.2, the decay (blue) or the buildup (green) of the hydride signal is obtained. The total experimental duration was 10 minutes. (b) Decay of the high-field hydride (black) and buildup of free H_2 (red) signals obtained with the pulse sequence sketched in Fig. 2b, plotted as a function of the exchange/relaxation period Δ. The experiment monitors the decay of the longitudinal magnetization of the hydrides or the hydrides' dissociation during Δ. Eight scans were measured for each spectrum, for a total experimental duration of 20 minutes. Both experiments were recorded using a solution of 0.8 mM metal complex, 15 mM mtz, 50 μM isoquinoline dissolved in methanol-d_4 in the presence of 5 bar 51% enriched p-H_2 at 25 °C.

Figure 4 displays the fitting of the experimental data, together with the optimized values of kinetic constants and relaxation rates. Errors associated to the fitting parameters were estimated by the Jackknife method (Caceci, 1989). Note that the fitting was performed without constraining any parameter. Nevertheless, the obtained value for the recovery rate for H_2 (0.62 ± 0.02 s^{-1}) is in good agreement with the one measured for the same sample performing a saturation-recovery experiment (0.603 ± 0.003 s^{-1}). Similarly, the experimental value of the decay rate for p-H_2 (0.226 ± 0.003 s^{-1}) is consistent with the result obtained from this fitting (0.20 ± 0.01 s^{-1}).

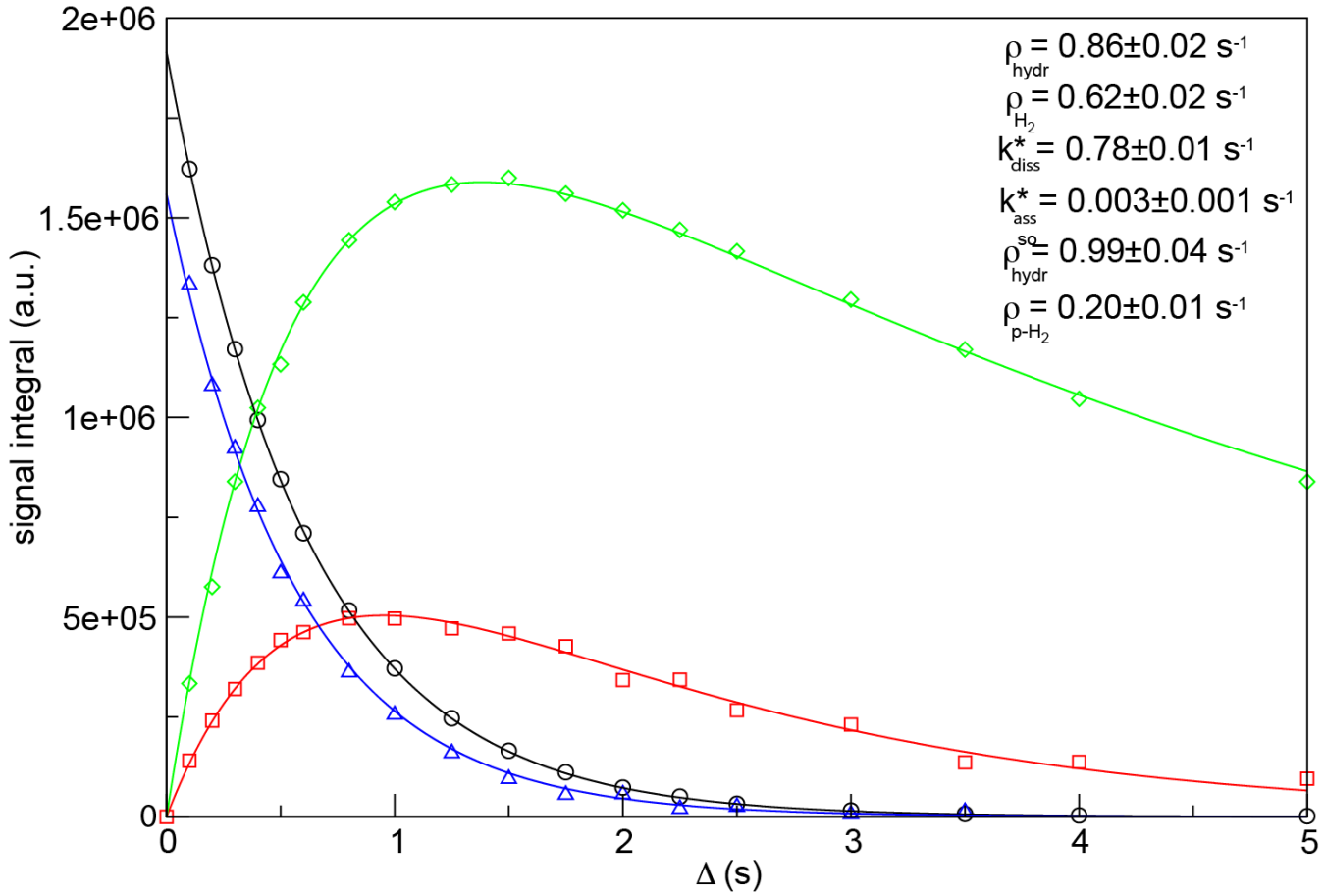

Figure 4. Simultaneous fit as a function of the relaxation period Δ of the signal integrals of hydrides and H_2 derived from the experimental data of Fig. 3, to determine the longitudinal magnetization decay rate (black circles), hydrides dissociation rate (red squares), p-H_2 association rate (green diamonds) and longitudinal spin order decay rate (blue triangles) in the asymmetric complex [Ir(IMes)$(H)_2$(IQ)$(mtz)_2$]Cl. The values of the hydrogen dissociation and association rate constants and the hydrogen/hydrides' relaxation rates are indicated. The experimental data and the fitting curves have been rescaled to the same number of scans for this plot.

As previously stated, the values of hydrogen dissociation/association rates reflect a multi-step process and, therefore, a detailed knowledge of the kinetic mechanism is necessary for their interpretation. However, the value of 0.78 s^{-1} here determined for the hydrogen dissociation rate constant indicates a relatively long lifetime of the $[Ir(IMes)(H)_2(IQ)(mtz)_2]^+$ asymmetric complex. This time stability seems to be a common feature of asymmetric complexes involving mtz as co-substrate, a positive aspect for PHIP chemosensing applications in complex mixture analysis, in which high-resolution 2D NMR spectra are necessary to resolve highly crowded regions. Thanks to the stability of these mtz complexes, we have been able to acquire well-resolved signals of low concentrated metabolites in urine extracts, using 2D PHIP-NMR spectra with evolution times exceeding 500 ms (Sellies et al., 2019). However, it should be mentioned that such high-resolution comes at

the cost of lower PHIP enhancements, due to a reduced p-H_2 refreshment rate. Therefore, a different co-substrate should be favored if maximal sensitivity is required.

5 Conclusions

We have presented an efficient approach for the experimental determination of the relaxation rates and kinetic parameters for p-H_2 association/dissociation in asymmetric PHIP complexes. The proposed PHIP-NMR experiments were tested for the substrate isoquinoline in combination with mtz as co-substrate and Ir-IMes as metal complex. We have thereby demonstrated that, thanks to the signal enhancement provided by PHIP, these NMR experiments can be efficiently employed even at low micromolar complex concentrations. Together with our recently published PHIP experiments to probe the substrate kinetics and relaxation rates (Hermkens et al., 2017), detailed experimental characterization of the parameters underlying PHIP signal enhancements can now be obtained for substrates at low µM concentrations. We believe that access to these parameters might help understanding the variations in PHIP enhancements for different substrates. Furthermore, it could guide a rational design of new PHIP-catalysts as well as the choice for the optimal co-substrate for the desired application.

Appendix A

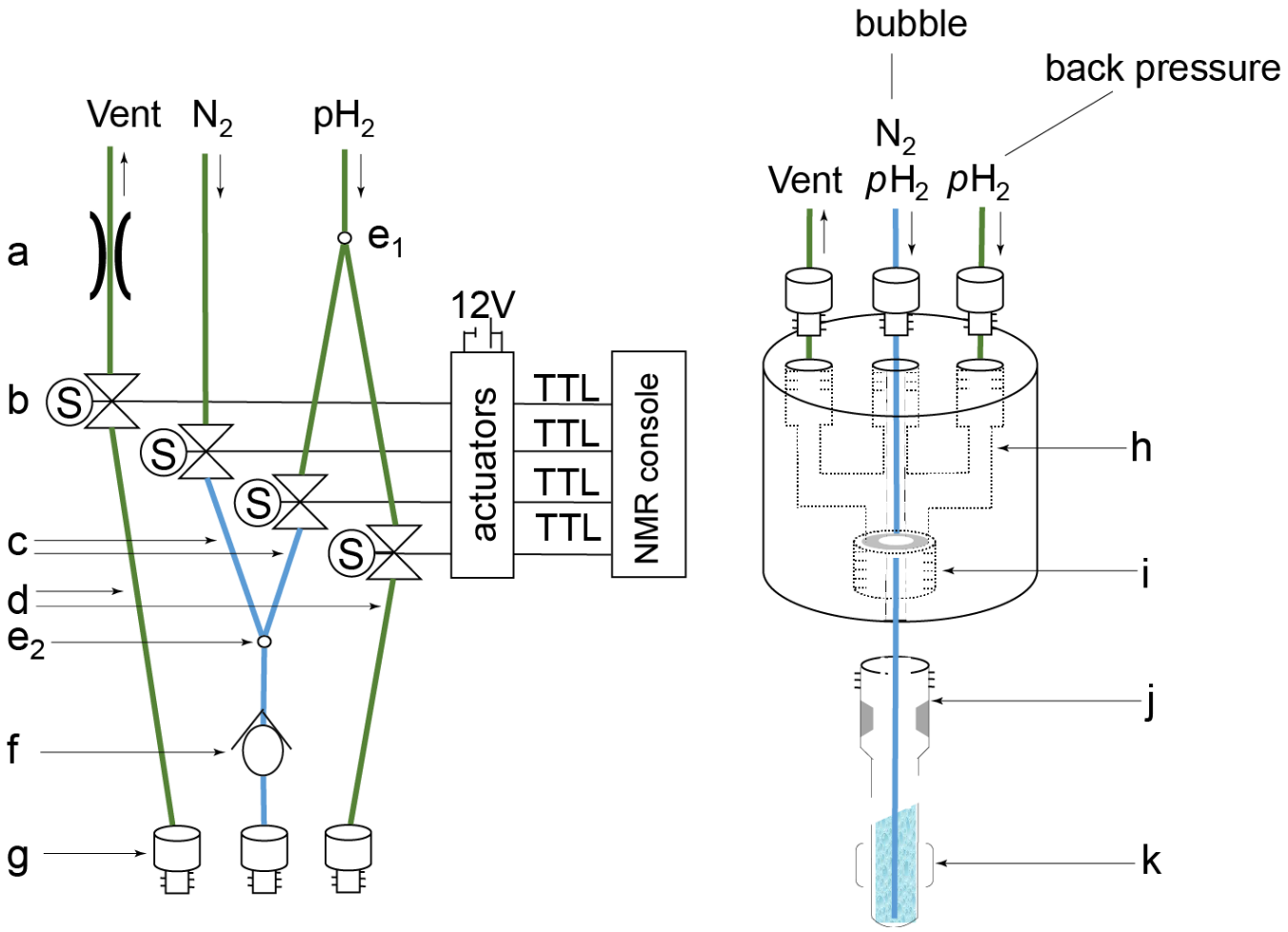

Figure A1. Schematic representation of the gas-liquid reaction set-up. Left: (a) variable pressure relief valve, set to 4 bar; (b) solenoids valves controlled via TTL-lines powered by an external 12 V source and timed via trigger commands in the pulse sequence taking care of controlled supply of nitrogen and para-hydrogen as described in section 2.2 and 2.3; (c) 1/16" O.D. PEEK tubing with 0.010" I.D. (blue); (d) 1/16" O.D. PEEK tubing with 0.030" I.D. (green); (e) Y-splitter: (e_1) splitting 5 bar p-H_2 source into a 'bubble' and a 'back pressure' line, (e_2) combining 5 bar N_2- and p-H_2-source into a joined bubble line; (f) check-valve; (g) tube fittings UNF 10-32 connectors. Right: (h) headpiece connecting the PEEK tubing holding the 7" thin wall QPV NMR tube; (i) UNF 7/16-20 thread holding the QPV NMR tube - using a 2 mm silicon disc on top of the tube to close off the system; (j) Wilmad 7" thin wall QPV NMR tube; (k) area of detection with the bubble line centered down to the bottom of the NMR tube.

Appendix B

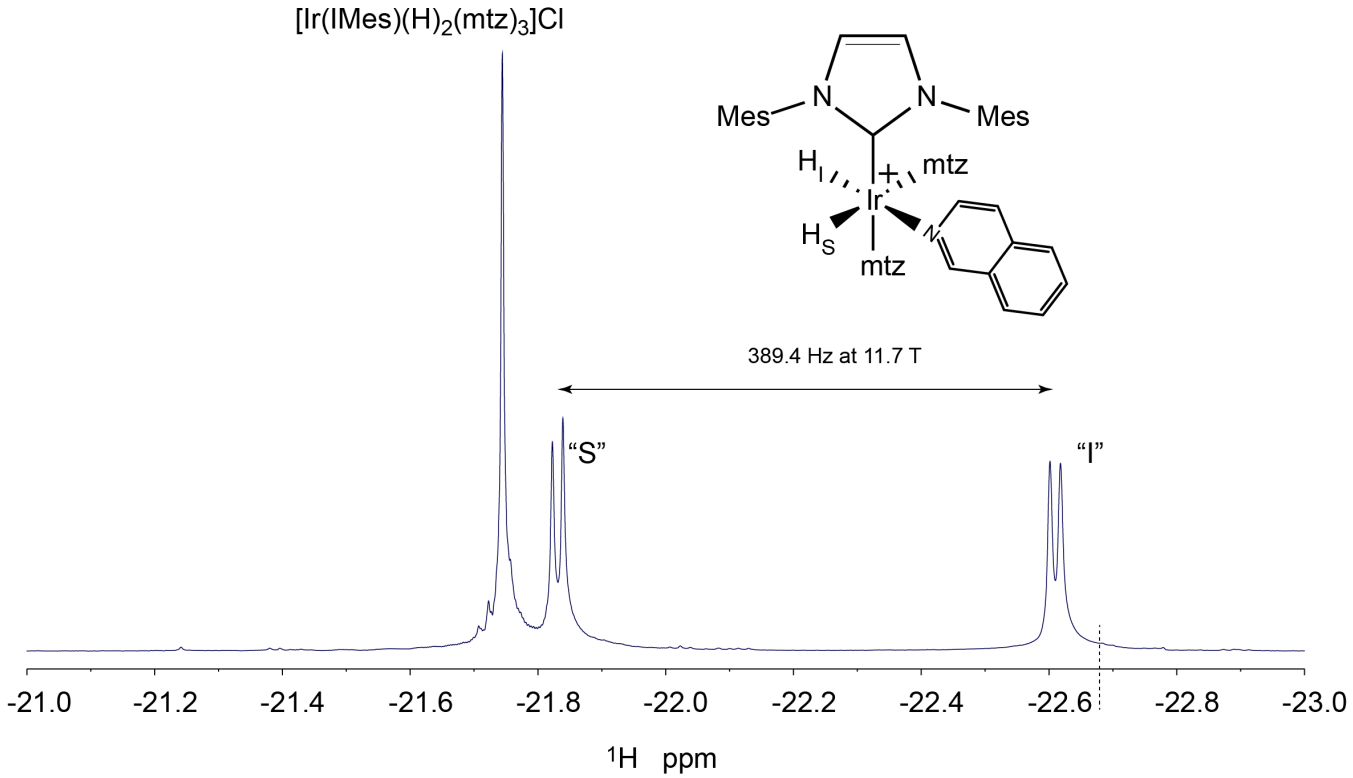

Figure B1. PHIP-NMR spectrum of the hydrides region of a solution of isoquinoline 50 μM, iridium-IMes complex 0.8 mM, mtz 15 mM in methanol-d_4 in the presence of 5 bar 51% enriched p-H_2. The experiment was recorded with 16 scans at 25 °C using a SEPP pulse sequence on an Agilent Unity Inova NMR spectrometer operating at 500 MHz, proton resonance frequency. The structure of the asymmetric complex formed by mtz and isoquinoline is indicated, together with the assignment of the two hydrides. The frequency difference between the two hydrides signals at 500 MHz is reported. The dotted line in proximity of the signal of hydride "I" indicates the selective excitation frequency for the hydrides employed in the kinetics experiments described in section 3.1.

Data availability

Experimental data are uploaded as supplemental data.

Author contributions

LS contributed to the theory section and the preparation of the manuscript, RLEGA prepared the NMR sample and the experimental setup for PHIP, MT conceived the project, acquired and analyzed the data and contributed in writing the manuscript.

Competing interests

The authors declare that they have no conflict of interest.

Special issue statement

This article is part of the special issue “Robert Kaptein Festschrift”. It is not associated with a conference.

Acknowledgements

The authors would like to thank prof. Floris Rutjes and prof. Martin Feiters, Synthetic Organic Chemistry Department (IMM, Radboud University) for providing mtz and the iridium-IMes complex employed in this work.

References

Adams, R. W., Aguilar, J. A., Atkinson, K. D., Cowley, M. J., Elliott, P. I., Duckett, S. B., Green, G.G., Khazal, I.G., López-Serrano, J. and Williamson, D.C.: Reversible interactions with para-hydrogen enhance NMR sensitivity by polarization transfer, Science, 323,1708-1711, https://doi.org/10.1126/science.1168877, 2009.

Appleby, K. M., Mewis, R. E., Olaru, A. M., Green, G. G., Fairlamb, I. J., and Duckett, S. B.: Investigating pyridazine and phthalazine exchange in a series of iridium complexes in order to define their role in the catalytic transfer of magnetisation from para-hydrogen, Chem. Sci., 6, 3981-3993, https://doi.org/10.1039/c5sc00756a, 2015.

Ardenkjær-Larsen, J. H., Fridlund, B., Gram, A., Hansson, G., Hansson, L., Lerche, M. H., Servin, R., Thaning, M. and Golman, K.: Increase in signal-to-noise ratio of >10,000 times in liquid-state NMR, Proc. Natl. Acad. Sci. U.S.A., 100, 10158-10163, https://doi.org/10.1073/pnas.1733835100, 2003.

Balacco, G., Marino, C. (2005) http://www.inmr.net/ (accessed Feb 1, 2016).

Barskiy, D. A., Knecht, S., Yurkovskaya, A. V., and Ivanov, K. L.: SABRE: Chemical kinetics and spin dynamics of the formation of hyperpolarization, Prog. Nucl. Magn. Reson. Spectrosc., 114, 33-70, https://doi.org/10.1016/j.pnmrs.2019.05.005, 2019.

Barskiy, D. A., Pravdivtsev, A. N., Ivanov, K. L., Kovtunov, K. V., and Koptyug, I. V.: A simple analytical model for signal amplification by reversible exchange (SABRE) process, Phys. Chem. Chem. Phys., 18, 89-93, https://doi.org/10.1039/c5cp05134g, 2016.

Bordonali, L., Nordin, N., Fuhrer, E., MacKinnon, N., and Korvink, J. G.: Parahydrogen based NMR hyperpolarisation goes micro: an alveolus for small molecule chemosensing, Lab Chip, 19, 503-512, https://doi.org/10.1039/c8lc01259h, 2019.

Bowers, C. R., and Weitekamp, D. P.: Parahydrogen and synthesis allow dramatically enhanced nuclear alignment. J. Am. Chem. Soc., 109, 5541-5542, https://doi.org/10.1021/ja00252a049, 1987.

Buljubasich L., Franzoni M.B., Münnemann K.: Parahydrogen Induced Polarization by Homogeneous Catalysis: Theory and Applications, in: Hyperpolarization Methods in NMR Spectroscopy. Topics in Current Chemistry, vol. 338, edited by Kuhn L., Springer, Berlin, Heidelberg, https://doi.org/10.1007/128_2013_420, 2013.

Caceci, M. S.: Estimating error limits in parametric curve fitting, Anal. Chem., 61, 2324-2327, https://doi.org/10.1021/ac00195a02, 1989.

Cowley, M. J., Adams, R. W., Atkinson, K. D., Cockett, M. C., Duckett, S. B., Green, G. G., Lohman, J.A.B., Kerssebaum, R., Kilgour, D. and Mewis, R. E.: Iridium N-heterocyclic carbene complexes as efficient catalysts for magnetization transfer from para-hydrogen, J. Am. Chem. Soc., 133, 6134-6137, https://doi.org/10.1021/ja200299u, 2011.

Delaglio, F., Grzesiek, S., Vuister, G.W., Zhu, G., Pfeifer, J., Bax, A.: NMRPipe: A multidimensional spectral processing system based on UNIX pipes, J. Biomol. NMR, 6, 277-293, https://doi.org/10.1007/bf00197809, 1995.

Eaton, J. W., Bateman, D., Hauberg, S. (2009) Gnu Octave Version 3.0.1 Manual: A High-Level Interactive Language for Numerical Computations 1st Edition.

Eshuis, N., Aspers, R. L., van Weerdenburg, B. J., Feiters, M. C., Rutjes, F. P., Wijmenga, S. S., and Tessari, M.: 2D NMR trace analysis by continuous hyperpolarization at high magnetic field, Angew. Chem. Int. Ed., 54,14527-14530, https://doi.org/10.1002/anie.201507831, 2015.

Eshuis, N., Hermkens, N., van Weerdenburg, B. J., Feiters, M. C., Rutjes, F. P., Wijmenga, S. S., and Tessari, M.: Toward nanomolar detection by NMR through SABRE hyperpolarization, J. Am. Chem. Soc., 136, 2695-2698, https://doi.org/10.1021/ja412994k, 2014.

Feng, B., Coffey, A. M., Colon, R. D., Chekmenev, E. Y., and Waddell, K. W.: A pulsed injection parahydrogen generator and techniques for quantifying enrichment, J. Magn. Reson., 214, 258-262, https://doi.org/10.1016/j.jmr.2011.11.015, 2012.

Gemeinhardt, M. E., Limbach, M. N., Gebhardt, T. R., Eriksson, C. W., Eriksson, S. L., Lindale, J. R., Goodson, E.A.,Warren, W.S., Chekmenev, E.Y. and Goodson, B. M.: "Direct" ^{13}C Hyperpolarization of ^{13}C-Acetate by MicroTesla NMR Signal Amplification by Reversible Exchange (SABRE), Angew. Chem. Int. Ed., 59, 418-423, https://doi.org/10.1002/anie.201910506, 2020.

Hermkens, N. K., Eshuis, N., van Weerdenburg, B. J., Feiters, M. C., Rutjes, F. P., Wijmenga, S. S., and Tessari, M.: NMR-based chemosensing via p-H_2 hyperpolarization: application to natural extracts, Anal. Chem., 88, 3406-3412, https://doi.org/10.1021/acs.analchem.6b00184, 2016.

Hermkens, N. K., Feiters, M. C., Rutjes, F. P., Wijmenga, S. S., and Tessari, M.: High field hyperpolarization-EXSY experiment for fast determination of dissociation rates in SABRE complexes, J. Magn. Reson., 276, 122-127, https://doi.org/10.1016/j.jmr.2017.01.011, 2017.

Hermkens, N. K., Aspers, R. L., Feiters, M. C., Rutjes, F. P., and Tessari, M.: Trace analysis in water-alcohol mixtures by continuous p-H_2 hyperpolarization at high magnetic field, Magn. Reson. Chem., 56, 633-640, https://doi.org/10.1002/mrc.4692, 2018.

Iali, W., Rayner, P. J., Alshehri, A., Holmes, A. J., Ruddlesden, A. J. and Duckett, S. B.: Direct and indirect hyperpolarisation of amines using parahydrogen, Chem. Sci., 9, 3677-3684, https://doi.org/10.1039/C8SC00526E, 2018.

Iali, W., Roy, S. S., Tickner, B. J., Ahwal, F., Kennerley, A. J., and Duckett, S. B.: Hyperpolarising pyruvate through signal amplification by reversible exchange (SABRE), Angew. Chem. Int. Ed., 58, 10271-10275, https://doi.org/10.1002/anie.201905483, 2019.

Kelly III, R. A., Clavier, H., Giudice, S., Scott, N. M., Stevens, E. D., Bordner, J., Samardjiev, I., Hoff, C.D., Cavallo, L., and Nolan, S. P.: Determination of N-heterocyclic carbene (NHC) steric and electronic parameters using the [(NHC)Ir($CO)_2$Cl] system, Organometallics, 27, 202-210, https://doi.org/10.1021/om701001g, 2008.

Logan, A. W. J., Theis, T., Colell, J. F. P., Warren, W. S. and Malcolmson, S. J.: Hyperpolarization of Nitrogen-15 Schiff Bases by Reversible Exchange Catalysis with para-Hydrogen, Chem. - A Eur. J., 22, 10777-10781, https://doi.org/10.1002/chem.201602393, 2016.

Mewis, R. E., Green, R. A., Cockett, M. C. R., Cowley, M. J., Duckett, S. B., Green, G. G. R., John, R. O., Rayner, P. J. and Williamson, D. C.: Strategies for the Hyperpolarization of Acetonitrile and Related Ligands by SABRE, J. Phys. Chem. B, 119, 1416-1424, https://doi.org/10.1021/jp511492q, 2015.

Pravica, M. G., and Weitekamp, D. P.: Net NMR alignment by adiabatic transport of parahydrogen addition products to high magnetic field, Chem. Phys. Lett., 145, 255-258, https://doi.org/10.1016/0009-2614(88)80002-2, 1988.

Rayner, P. J., and Duckett, S. B.: Signal amplification by reversible exchange (SABRE): From discovery to diagnosis, Angew. Chem. Int. Ed., 57, 6742-6753, https://doi.org/10.1002/anie.201710406, 2018.

Rayner, P. J., Burns, M. J., Olaru, A. M., Norcott, P., Fekete, M., Green, G. G., Louise A. R. Highton, L.A.R., Mewis, R.E., and Duckett, S. B.: Delivering strong ^{1}H nuclear hyperpolarization levels and long magnetic lifetimes through signal amplification by reversible exchange, Proc. Natl. Acad. Sci. U.S.A., 114, E3188-E3194, https://doi.org/10.1073/pnas.1620457114, 2017.

Reile, I., Eshuis, N., Hermkens, N. K. J., Van Weerdenburg, B. J. A., Feiters, M. C., Rutjes, F. P. J. T., and Tessari, M.: NMR detection in biofluid extracts at sub-μM concentrations via para-H_2 induced hyperpolarization, Analyst, 141, 4001-4005, https://doi.org/10.1039/C6AN00804F, 2016.

Shchepin, R.V., Barskiy, D.A., Coffey, A. M., Goodson, B. M. and Chekmenev, E. Y.: NMR Signal Amplification by Reversible Exchange of Sulfur-Heterocyclic Compounds Found In Petroleum, ChemistrySelect, 1, 2552-2555, http://dx.doi.org/10.1002/slct.201600761, 2016.

Seefeld, M.A., Rouse, M.B., Heerding, D.A., Peace, S., Yamashita, D.S., McNulty, K.C, Inhibitors of AKT Activity, WO 2008/098104 A1, 14 August 2008.

Sellies, L., Reile, I., Aspers, R. L., Feiters, M. C., Rutjes, F. P., and Tessari, M.: Parahydrogen induced hyperpolarization provides a tool for NMR metabolomics at nanomolar concentrations, Chem. Commun., 55, 7235-7238, https://doi.org/10.1039/c9cc02186h, 2019.

Sengstschmid, H., Freeman, R., Barkemeyer, J., and Bargon, J.: A new excitation sequence to observe the PASADENA effect, J. Magn. Reson., Ser. A, 120, 249-257, https://doi.org/10.1006/jmra.1996.0121, 1996.

Stanbury, E. V., Richardson, P. M., and Duckett, S. B.: Understanding substrate substituent effects to improve catalytic efficiency in the SABRE hyperpolarisation process Catal. Sci. Technol., 9, 3914-3922, https://doi.org/10.1039/c9cy00396g, 2019.

Theis, T., Ortiz, G. X., Logan, A. W. J., Claytor, K. E., Feng, Y., Huhn, W. P., Blum, V., Malcolmson, S. J., Chekmenev, E. Y., Wang, Q. and Warren, W. S.: Direct and cost-efficient hyperpolarization of long-lived nuclear spin states on universal $^{15}N_2$-diazirine molecular tags, Sci. Adv., 2, e1501438, https://doi.org/10.1126/sciadv.1501438, 2016.

Theis, T., Truong, M. L., Coffey, A. M., Shchepin, R. V., Waddell, K. W., Shi, F., Goodson, B.M., Warren, W.S., and Chekmenev, E. Y.: Microtesla SABRE enables 10% nitrogen-15 nuclear spin polarization, J. Am. Chem. Soc., 137, 1404-1407, https://doi.org/10.1021/ja512242d, 2015.

Walker, T. G., and Happer, W.: Spin-exchange optical pumping of noble-gas nuclei, Rev. Mod. Phys., 69, 629-642, https://doi.org/10.1103/revmodphys.69.629, 1997.

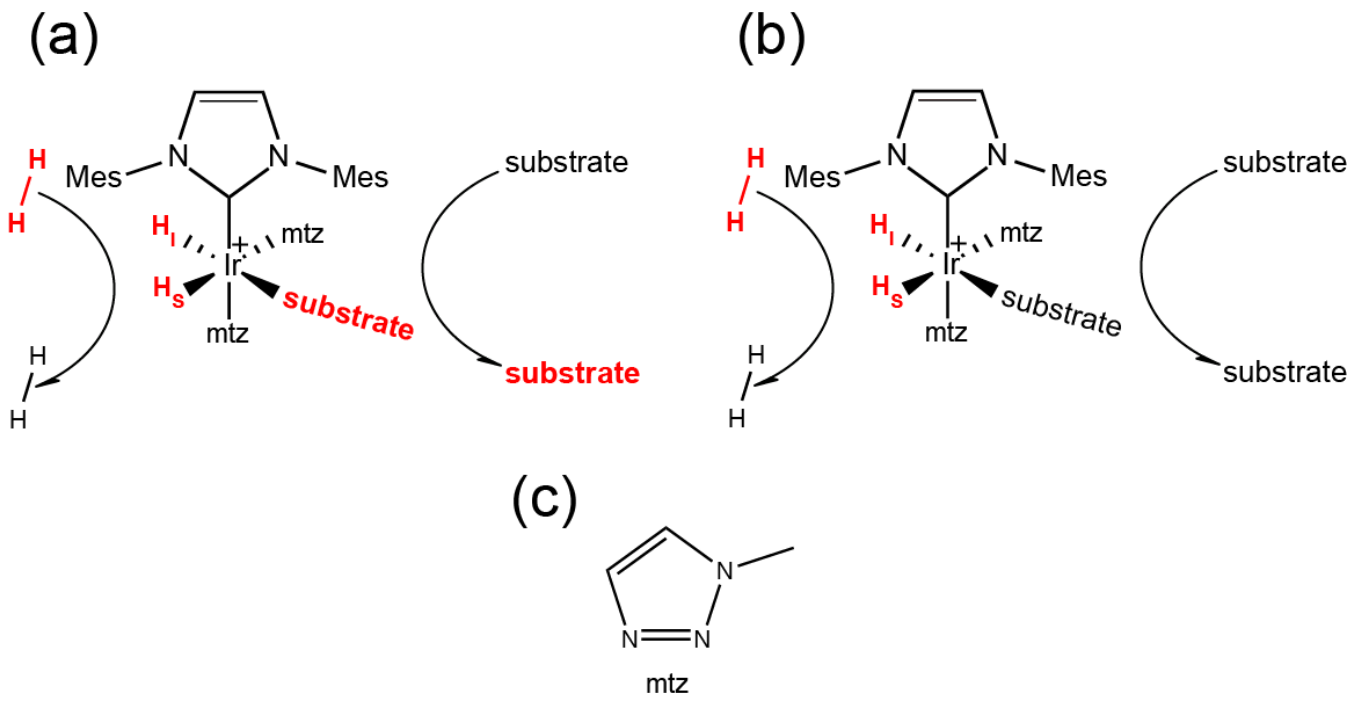

Figure 1: (a) Schematic representation of the SABRE experiment at low magnetic field: spontaneous transfer of spin order from the hydrides originating from p-H_2 to the substrate nuclear spins occurs via the scalar coupling network within the transient complex [Ir(IMes)$(H)_2$(substrate)$(mtz)_2$]Cl. The subsequent dissociation of the substrate produces hyperpolarized molecules in solution that can be detected by NMR with enhanced sensitivity. SABRE hyperpolarization has been demonstrated for different classes of compounds (e.g. nitrogen (Adams et al., 2009) and sulphur (Shchepin et al., 2016) heteroaromatic compounds, nitriles (Mewis et al., 2015), amines (Iali et al., 2018), Schiff bases (Logan et al., 2016) and diazirines (Theis et al., 2016)). (b) Schematic representation of PHIP at high magnetic field: formation of the asymmetric complex [Ir(IMes)$(H)_2$(substrate)$(mtz)_2$]Cl due to the reversible association of p-H_2 and substrates produces longitudinal spin order of the hydrides, which can be revealed by NMR signals that are enhanced up to three orders of magnitude compared to thermal measurements on a conventional high field spectrometer. (c) Structure of the mtz co-substrate (1-methyl-1,2,3-triazole).

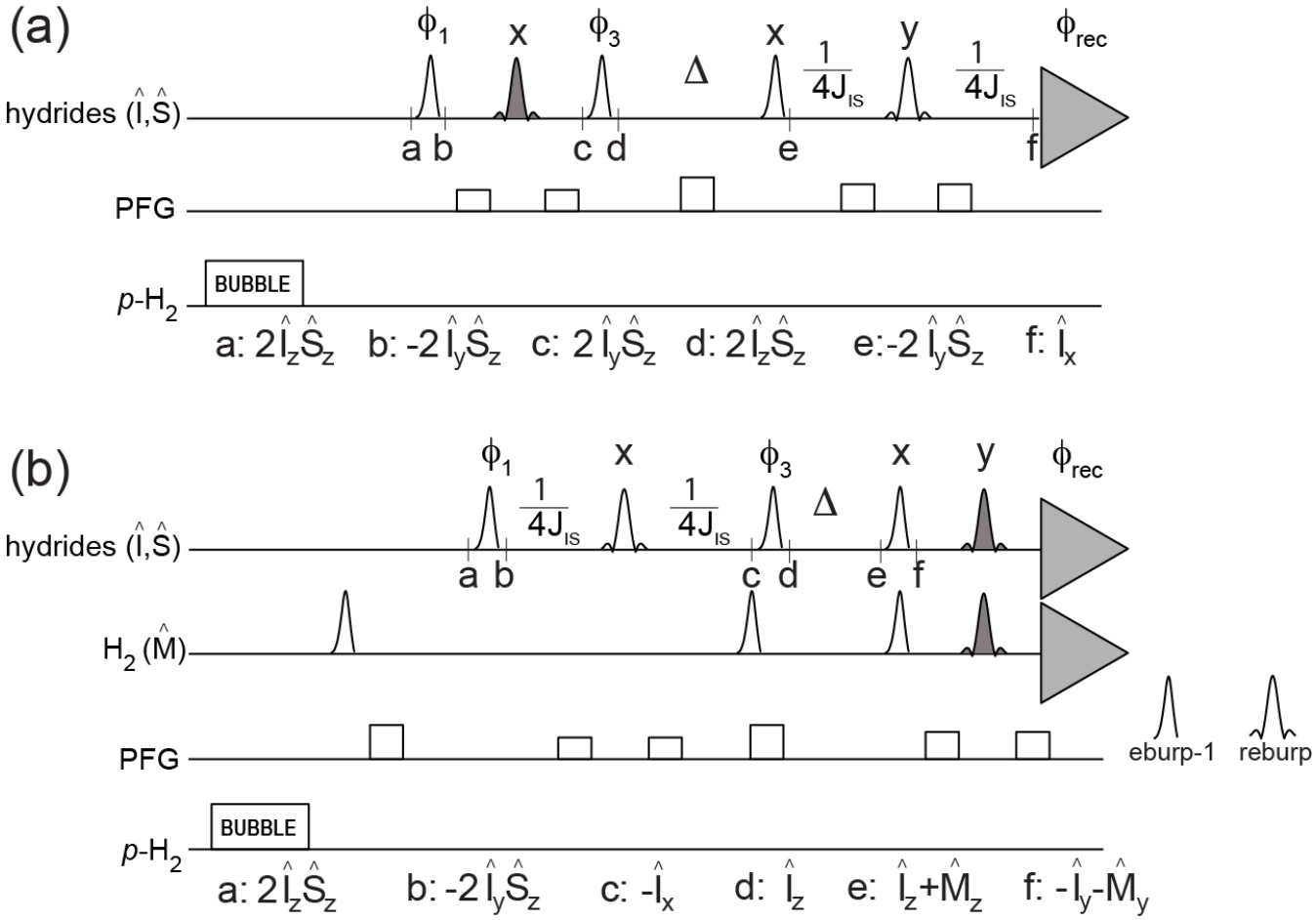

Figure 2. Pulse sequences to measure relaxation and kinetic parameters for hydrides in asymmetric complexes. The transmitter offset is placed at -11.35 ppm, and the spectral region between -31.36 ppm and 8.66 ppm is acquired. Open shaped profiles indicate selective off-resonance pulses *eburp-1* (for excitation of the high-field hydride, 500 Hz bandwidth) or *reburp* (for refocusing, 2000 Hz bandwidth). Filled *reburp* pulses cover a smaller bandwidth (500 Hz) for the hydrogen and/or the high-field hydride resonance. Individual scans are stored separately and recombined during processing so that different pathways can be selected. J_{IS} indicates the inter-hydrides scalar coupling constant (8.2 Hz). (a) Pulse scheme to measure the decay rate of hydrides' longitudinal spin order as well as association of p-H_2 to the iridium complex. The following phase cycle is employed: ϕ_1 = x,-x; ϕ_3 = x,x,-x,-x; ϕ_{rec} = x. (b) Pulse scheme to measure the decay rate of hydrides' longitudinal magnetization as well as hydrides dissociation from the complex. The following phase cycle is employed: ϕ_1 = x,-x; ϕ_3 = y,y,-y,-y; ϕ_{rec} = x,-x,-x,x. H_2 longitudinal magnetization is suppressed at the start of the pulse sequence by selective 90-degree pulses after the bubbling period and at the beginning of the relaxation period Δ. The final excitation/spin-echo before acquisition selectively excites/refocuses both the magnetization from H_2 and from the high-field hydride. In other words, the last excitation/refocusing pulses consist of the superposition of two *eburp-1*/*reburp* pulses, for the selective detection of the high-field hydride as well as the hydrogen resonances.

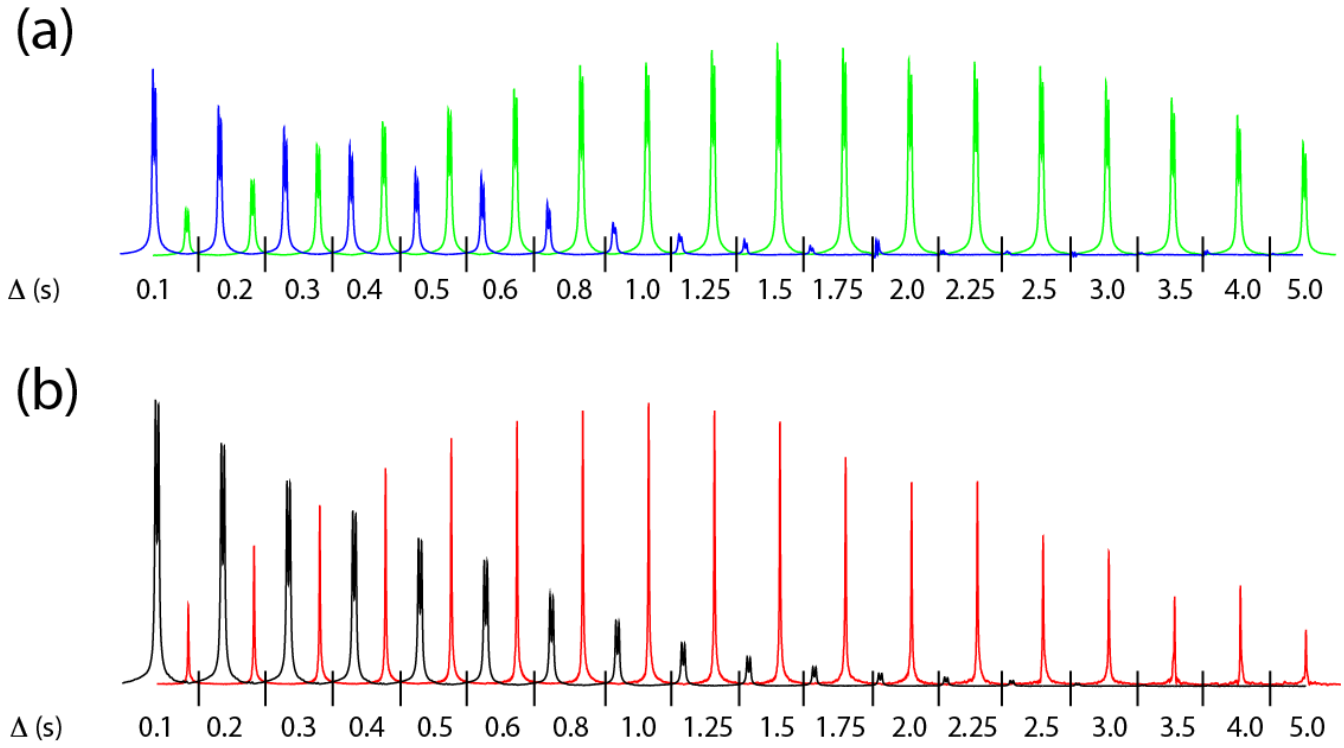

Figure 3. (a) High-field hydride signals obtained with the pulse sequence sketched in Fig. 2a, plotted as a function of the exchange/relaxation period Δ. The experiment monitors the decay of the longitudinal spin order of the hydrides or the association of p-H_2 to the complex during Δ. By taking different combinations of four FIDs as reported in Sec. 3.2, the decay (blue) or the buildup (green) of the hydride signal is obtained. The total experimental duration was 10 minutes. (b) Decay of the high-field hydride (black) and buildup of free H_2 (red) signals obtained with the pulse sequence sketched in Fig. 2b, plotted as a function of the exchange/relaxation period Δ. The experiment monitors the decay of the longitudinal magnetization of the hydrides or the hydrides' dissociation during Δ. Eight scans were measured for each spectrum, for a total experimental duration of 20 minutes. Both experiments were recorded using a solution of 0.8 mM metal complex, 15 mM mtz, 50 μM isoquinoline dissolved in methanol-d_4 in the presence of 5 bar 51% enriched p-H_2 at 25 °C.

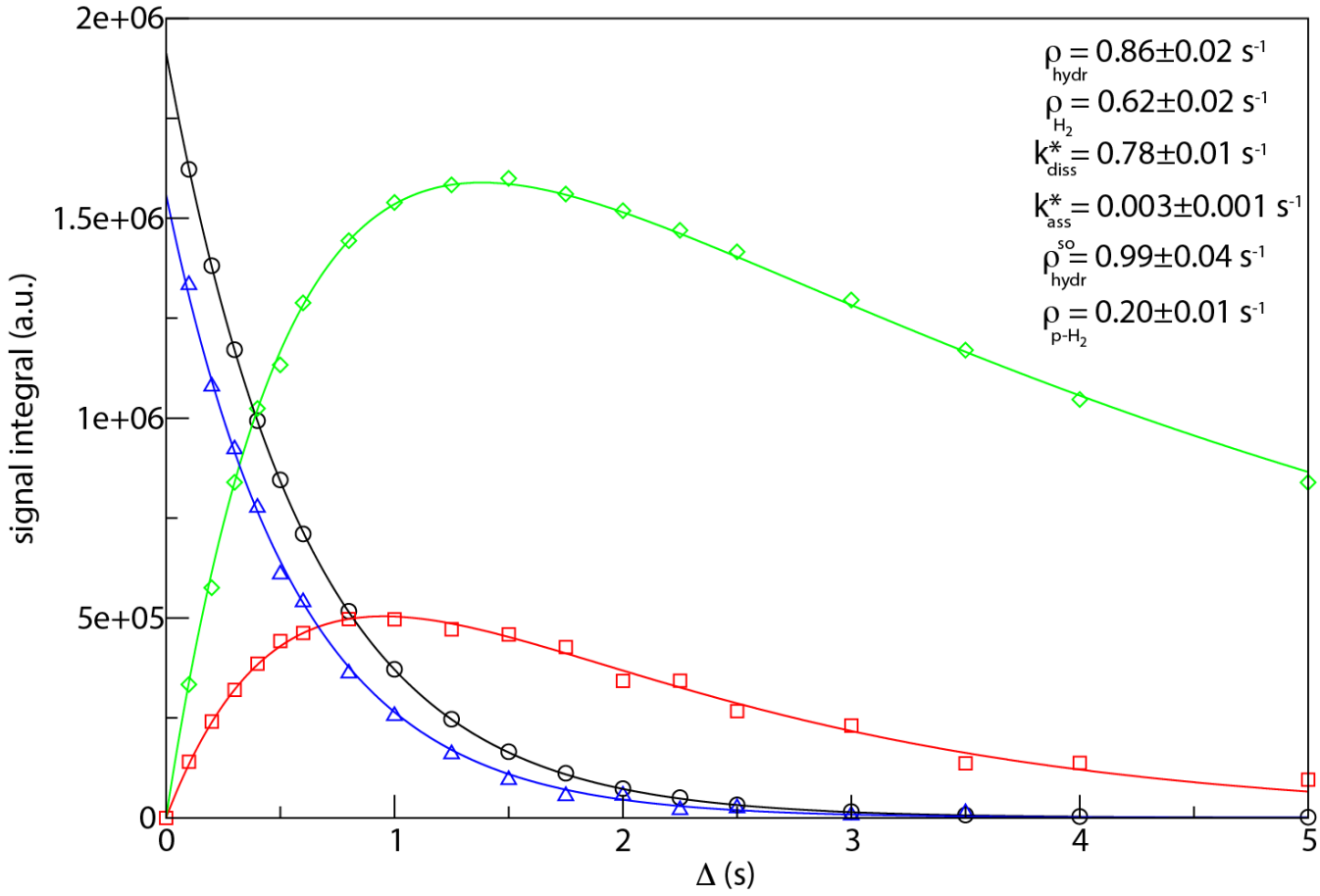

Figure 4. Simultaneous fit as a function of the relaxation period Δ of the signal integrals of hydrides and H_2 derived from the experimental data of Fig. 3, to determine the longitudinal magnetization decay rate (black circles), hydrides dissociation rate (red squares), p-H_2 association rate (green diamonds) and longitudinal spin order decay rate (blue triangles) in the asymmetric complex [Ir(IMes)$(H)_2$(IQ)$(mtz)_2$]Cl. The values of the hydrogen dissociation and association rate constants and the hydrogen/hydrides' relaxation rates are indicated. The experimental data and the fitting curves have been rescaled to the same number of scans for this plot.